A plant Shaker-like K^+ channel switches between two distinct gating modes resulting in either inward-rectifying or 'leak' current

Ingo Dreyer[1,2], Erwan Michard[2], Benoît Lacombe[3], Jean-Baptiste Thibaud*

Laboratoire de Biochimie et Physiologie Moléculaire des Plantes, UMR 5004, Agro-M/CNRS/INRA/UM2, Place Viala, 34060 Montpellier, Cedex 1, France

Received 12 July 2001; revised 31 July 2001; accepted 31 July 2001

First published online 27 August 2001

Edited by Maurice Montal

Abstract Among the Shaker-like plant potassium channels, AKT2 is remarkable because it mediates both instantaneous 'leak-like' and time-dependent hyperpolarisation-activated currents. This unique gating behaviour has been analysed in *Xenopus* oocytes and in COS and Chinese hamster ovary cells. Whole-cell and single-channel data show that (i) AKT2 channels display two distinct gating modes, (ii) the gating of a given AKT2 channel can change from one mode to the other and (iii) this conversion is under the control of post-translational factor(s). This behaviour is strongly reminiscent of that of the KCNK2 channel, recently reported to be controlled by its phosphorylation state. © 2001 Published by Elsevier Science B.V. on behalf of the Federation of European Biochemical Societies.

Key words: Potassium channel; Voltage-gating; Post-translational modification; Patch-clamp

1. Introduction

All Shaker-like plant K^+ channel α-subunits are characterised by a common structure, a hydrophobic core displaying six transmembrane segments (S1–S6) and a pore forming motif P between S5 and S6. The tetrameric channels they form, however, segregate into two channel sub-families according to the direction in which they transport K^+ ions. Inwardly-rectifying K^+ (K^+_{in}) Shaker channels like KAT1 [1–5], KAT2 [6], KST1 [7], AKT1 [8,9], SKT1 [10], ZMK1 [11] and LKT1 [12] are closed at membrane voltages less negative than about −80 mV. They open upon hyperpolarisation and thus mediate potassium uptake under physiological conditions. In contrast, outwardly-rectifying (K^+_{out}) Shaker channels like SKOR [13] and GORK [14] mediate K^+ efflux by closing upon hyperpolarisation and opening upon depolarisation.

In this context, the potassium channels AKT2 from *Arabidopsis thaliana* and ZMK2 cloned from *Zea mays* display a particular behaviour because they mediate both potassium influx and potassium efflux [15–20]. These channels, which share about 40% identity with K^+_{in} channels such as KAT1 and 27% with K^+_{out} channels such as SKOR, are characterised by an instantaneous, 'leak-like' potassium conductance which superimposes with a time-dependent component increasing in magnitude upon hyperpolarisation. This unique gating behaviour and its modulation are poorly understood, and therefore, their roles in the physiological activity of AKT2 and its homologues remain speculative.

2. Materials and methods

2.1. Expression of AKT2 in COS and Chinese hamster ovary (CHO) cells and in Xenopus oocytes

AKT2 cDNA was cloned in pCI (Promega, Madison, WI, USA) or pIRES [21], which allowed co-expression of AKT2 and the membrane protein CD8 [22].

COS-7 cells were cultured in Dulbecco's modified Eagle's medium (DMEM) (Gibco-BRL) complemented with 10% foetal bovine serum (Gibco-BRL) at 37°C in 5% CO_2. One day before transfection, cells were detached with trypsin–EDTA (Gibco-BRL) and transferred to 35-mm dishes (20 000 cells per dish). Per dish, 80 μl HBS 2× (NaCl 280 mM, HEPES 50 mM, Na_2HPO_4 15 mM, pH 7.15) were gently mixed with 80 μl TE–$CaCl_2$ (1 mM Tris–HCl, pH 8, EDTA 1 mM; $CaCl_2$ 250 mM) containing 1.5 μg pIRES-AKT2. The DNA precipitate was added to cells in their culture media. After 8 h, cells were rinsed twice with DMEM. Electrophysiological analysis was performed 3 or 4 days later.

CHO cells were cultured in the same conditions as COS cells (HT media supplement (Sigma) was added to culture media). The day before transfection, cells were detached with trypsin–EDTA and transferred to 35-mm dishes (160 000 cells per dish). Cells were then transfected with 1.5 μg pIRES-AKT2 DNA per plate using Fugene 6 reagent (Boehringer Mannheim) as described by the manufacturer. Electrophysiological analysis was performed 2 or 3 days later. Control experiments were performed on cells transfected with pIRES alone.

Xenopus oocytes (CRBM, CNRS, Montpellier, France) were injected with 20 ng (0.02 μl) of pCI-AKT2. Control oocytes were injected with 0.02 μl deionised water.

2.2. Electrophysiological recordings

Two-electrode voltage-clamp experiments on oocytes were carried out as previously described [23]. Patch-clamp experiments on oocytes (single-channel) and on COS and CHO cells (whole-cell) expressing AKT2 were carried out as previously described [17].

2.3. Tail-current analysis

In whole-cell experiments tail currents were recorded after the test pulse. They displayed a single-exponential time course as routinely checked with the fitting procedure featured by Clampfit software (version 6.4, Axon Instruments Inc., USA). All subsequent analyses were made on the initial value of the tail current sampled on the exponential fit and denoted i_0. The dependence of i_0 on the test-pulse voltage (E) was fitted by the following equation, which is a modified form of the classically used Boltzmann law:

$$i_0(E) = i_{0,\min} + (i_{0,\max} - i_{0,\min}) * [1/(1 + \exp[z * F/(R * T) * (E - E_{1/2})])]$$

*Corresponding author. Fax: (33)-499-612 930.
E-mail address: thibaud@ensam.inra.fr (J.-B. Thibaud).

[1] Present address: Universität Potsdam, Institut für Biochemie und Biologie, Abt. Molekularbiologie, Karl-Liebknecht-Str. 24/25, Haus 20, D-14476 Golm, Germany.
[2] These authors contributed equally to this work.
[3] Present address: Julius-von-Sachs-Institut für Biowissenschaften, Lehrstuhl Botanik I, Molekulare Pflanzenphysiologie und Biophysik, Julius-von-Sachs-Platz 2, D-97082 Würzburg, Germany.

0014-5793/01/$20.00 © 2001 Published by Elsevier Science B.V. on behalf of the Federation of European Biochemical Societies.
PII: S0014-5793(01)02832-0

where there are four adjustable parameters: $i_{0,max}$ and $i_{0,min}$, the values of maximum and minimum i_0, z, the apparent gating charge, and $E_{1/2}$, the half-activation potential. In the example of Fig. 2, data from five cells were pooled to yield the common z and $E_{1/2}$ values used for curves shown in Fig. 2C,D.

3. Results and discussion

3.1. AKT2 macroscopic current diversity

AKT2 macroscopic current was recorded (whole-cell configuration) in COS and CHO cells. Pulses of 1.6 s were applied from a holding potential of +40 mV to a voltage ranging from +60 mV (CHO) or +80 mV (COS) to −140 mV (steps of −20 mV). In the two systems, AKT2 currents displayed similar properties to those previously reported [17]: these currents showed a time- and voltage-dependent component in addition to an instantaneous (i.e. both time- and voltage-independent) component. Both components were routinely identified as K^+ currents, displaying reversal at E_K and block by Cs^+ ions (not shown, see ref. [17]) and were never observed in control cells (see Section 2). Intriguingly, the relative importance of the so-called leak current with respect to the total AKT2 current (this was arbitrarily calculated at −140 mV, expressed in % and hereafter denoted $r_{-140\,mV}$) was extremely variable. In 22 tested CHO cells (2 or 3 days after transfection) $r_{-140\,mV}$ varied from 0.68 to 73%. The $r_{-140\,mV}$ variation range extended from 22 to 94% in 56 tested COS cells (3 or 4 days after transfection). Sample records shown in Fig. 1A exemplify this fact: from left to right the $r_{-140\,mV}$ value (figured as the white portion of the bar aside current records, Fig. 1A) varied from 11 up to 84%. As a consequence of such a variation, the whole-cell current/voltage relationship at steady-state could vary from a strongly inward-rectifying pattern to an essentially leaky one: Fig. 1B shows AKT2 current from two COS cells of the same batch; for a similar current intensity, the $r_{-140\,mV}$ value is 22% in one cell, 94% in the other. In both COS- and CHO-expression systems, it was noticed that $r_{-140\,mV}$ increased with time 'post-transfection' (Fig. 1C), while the total AKT2 current tended to increase. For example, in CHO cells, total AKT2 current and $r_{-140\,mV}$ were -1.33 ± 0.21 nA and $22.9 \pm 6.0\%$ ($n = 12$) after 2 days and -3.08 ± 0.62 nA and $48.9 \pm 5.3\%$ ($n = 11$) after 3 days. In

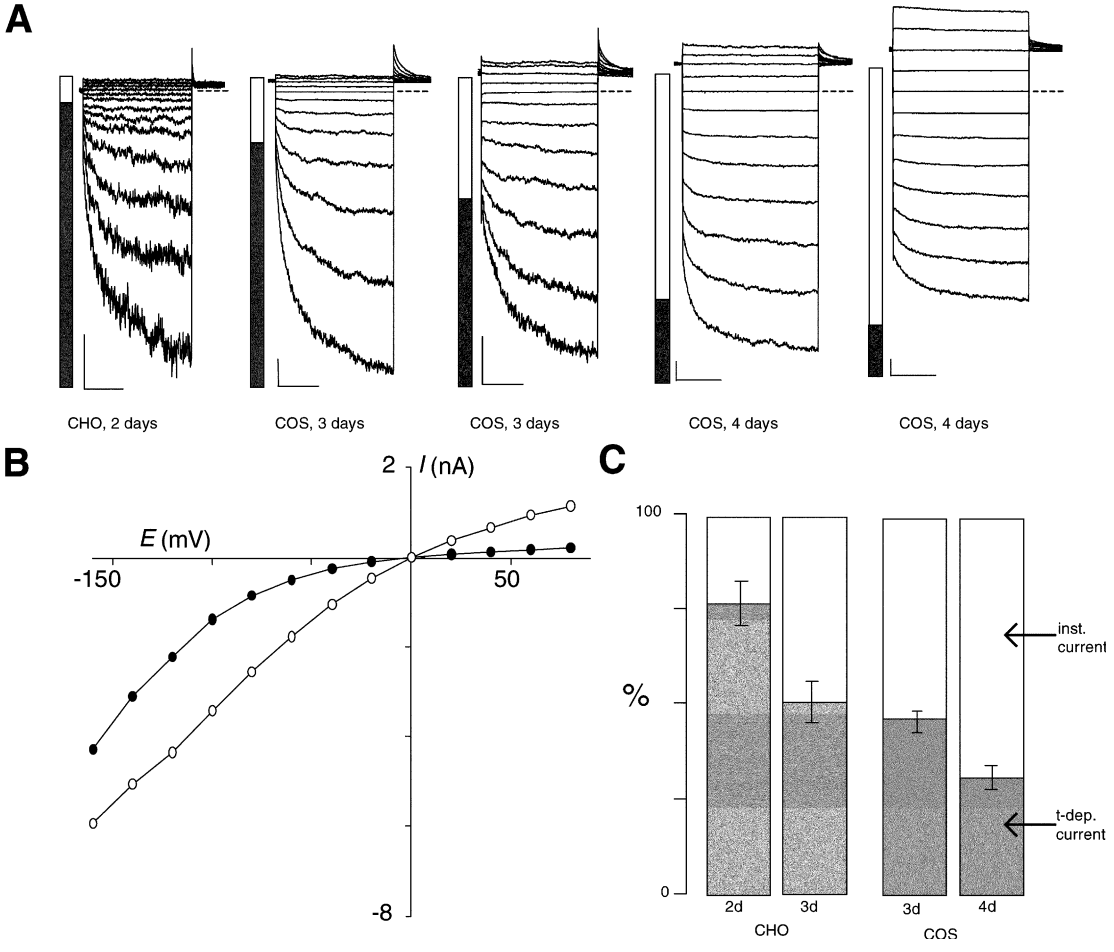

Fig. 1. Broad pattern of whole-cell currents recorded in COS or CHO cells expressing AKT2. A: Sample current records obtained in CHO or COS cells. Horizontal scale bar is 0.5 s and vertical one is 0.5 nA. Bar graphs at left of traces display the relative importance, at −140 mV, of time-dependent current (grey) and instantaneous current (white). B: Current/voltage (*I*/*E*) relationship at steady-state in two AKT2-expressing COS cells. These cells are from the same batch (3 days after transfection) and exemplify the variability of membrane rectification resulting from AKT2 expression. C: Increase of the relative importance at −140 mV (shown by the white section of bar graphs) of the instantaneous current with time after cell transfection. Data are shown as mean ± S.D. ($n = 5$). Bath solution contained (mM): KCl (150), $CaCl_2$ (1), $MgCl_2$ (1.5), HEPES/NaOH (10, pH 7.4); pipette solution contained (mM): KCl (150), $MgCl_2$ (1.5), EGTA (3), HEPES/NaOH (10, pH 7.2). Potassium equilibrium potential (E_K) is at 0 mV. From a holding potential of +40 mV, 1.6-s-long pulses were applied at voltages ranging from +60 mV (CHO) or +80 mV (COS) to −140 mV (20 mV steps).

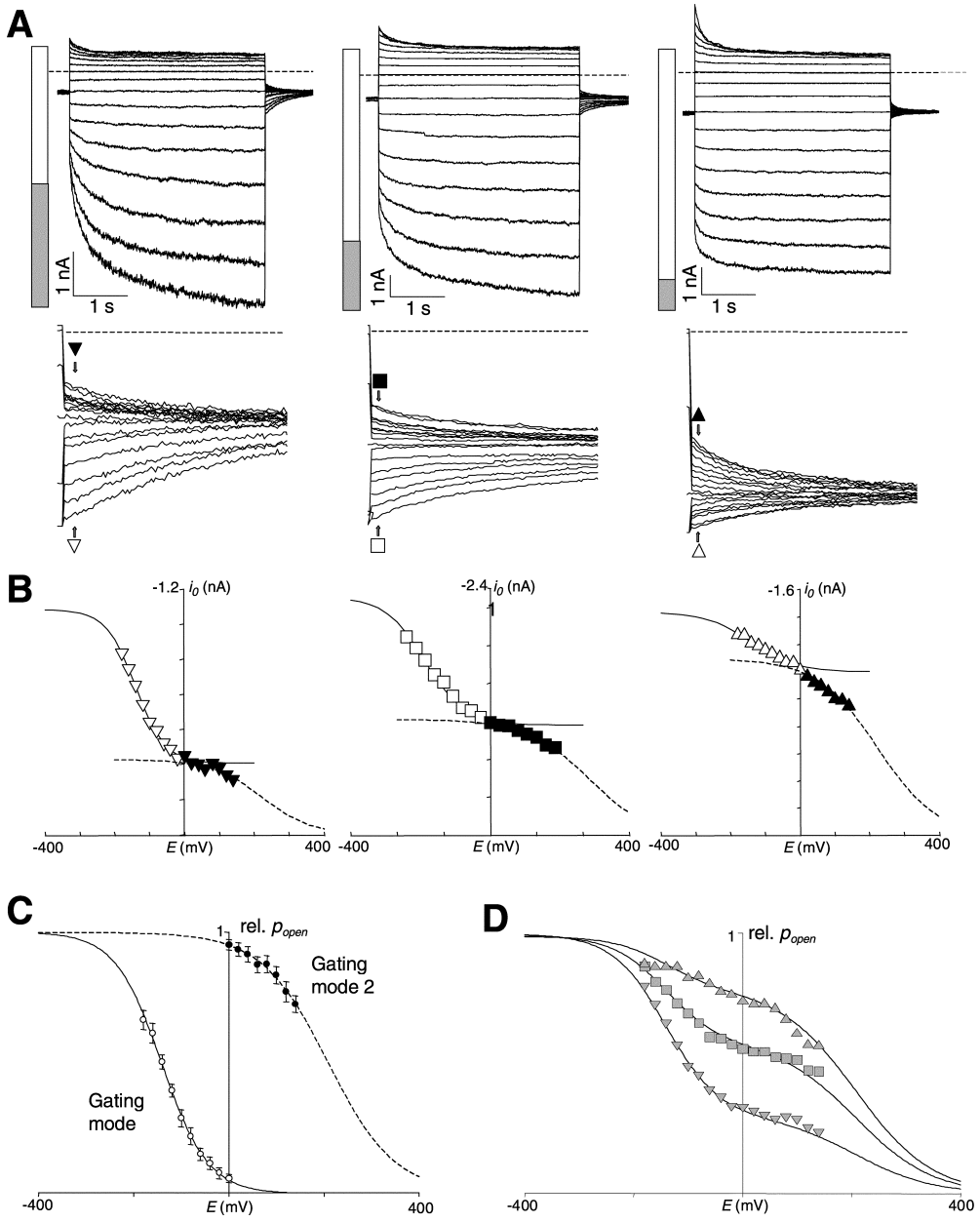

Fig. 2. Tail-currents analysis suggesting dual voltage-gating of AKT2 channels. A: Pulse and tail whole-cell AKT2 currents elicited by stimulation in the −180 to +140 mV range (example of three COS cells). Top: Horizontal scale bar is 1 s and vertical one is 1 nA. Bar graphs have the same meaning as in Fig. 1 (white area shows $r_{-140\,mV}$). Bottom: Tail currents are shown at larger scale below the whole records. Symbols (black or white, respectively, for i_0 resulting from pulses at positive or negative voltages) indicate the sampling-time of data (i_0) analysed in (B). Horizontal dashed lines in top and bottom graphs indicate the zero current level. B: Dependence of i_0 on test-pulse voltage. Data are from (A) with cross-referenced symbols. Parameters of two Boltzmann equations were adjusted (Marquardt–Levenberg algorithm, see Section 2) to fit separately the white and black point sets. The resulting curves are shown with plain and dashed lines respectively. C: Averaged dual Boltzmann curves obtained for five cells, as in (B). Data are shown as rel. p_{open} (mean ± S.D., $n = 5$) after normalisation of i_0 data. Left-hand/right-hand curve show, respectively, voltage-gating of type-1/type-2 AKT2 channels. D: Rel. p_{open} (E) curves resulting from combination of $(1-r_{abs.})$% type-1 and $r_{abs.}$% type-2 channels (see text). Parameters of the two Boltzmann components were from (C) and the value of $r_{abs.}$ was adjusted to fit normalised data from (B) (cross-referenced symbols). See Fig. 1 for bath and pipette solutions.

COS cells, between 3 and 4 days after transfection, the total AKT2 current increase (from −3.34 ± 0.99 nA to −5.01 ± 0.92 nA, $n = 11$) was, however, less than the increase of $r_{-140\,mV}$ (from 53.9 ± 2.9% to 68.7 ± 3.3%, $n = 17$).

3.2. May the AKT2 channel have two gating modes?

Neither the fact that a Shaker-like channel can enable some leak current to flow in addition to a time- and voltage-dependent one, nor the fact that the relative importance of this leak current (i.e. $r_{-140\,mV}$) can greatly vary are as yet understood. One hypothesis would be that two types of AKT2 channels were operating. The so-called type-1 AKT2 channels would behave as voltage-gated channels, while the so-called type-2 AKT2 channels would behave as open-leak channels. Among the three expression systems (CHO and COS cells, and *Xenopus* oocytes) in which this unexplained AKT2 behaviour was observed, the COS cell line we used was the one which withstood the more extended voltage range, with less endogenous

current. Exploring strongly positive values of membrane potential (up to +140 mV) revealed a slow current component ($\tau_{100\,mV} = 450$ ms) in AKT2-expressing COS cells, which was never observed in control cells. For example, upon a voltage step from −40 mV to +140 mV, the evoked current not only responded instantaneously to the altered electrochemical gradient but deactivated in a time- and voltage-dependent manner and, accordingly, the tail current recorded subsequently (i.e. upon a step back to −40 mV, see dashes and symbols in Fig. 2A) showed re-activation ($\tau = 280$ ms).

Currents recorded from three cells displaying $r_{-140\,mV}$ values of 53, 74 and 88% are shown in Fig. 2A. The amplitude of the time-dependent (deactivating) current recorded at strongly positive potential values increased with the relative importance of the leak current at −140 mV (i.e. the $r_{-140\,mV}$ value). In the framework of the hypothesis proposed above, this de-

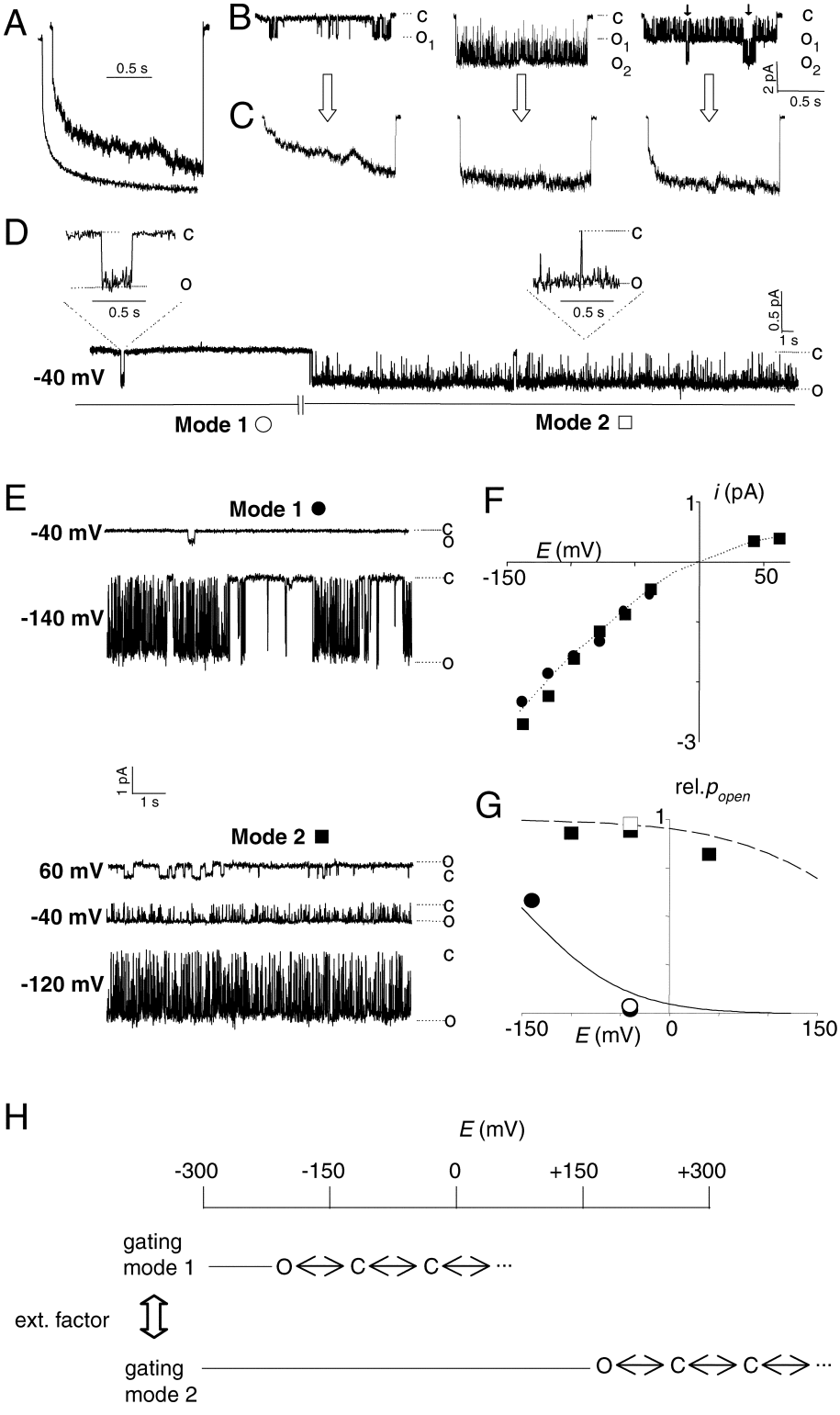

activating current could be ascribed to type-2 channels. By the same token, the current re-activating at −40 mV following pulses to positive potential values could be ascribed to type-2 channels (see enlargement of the tail currents in Fig. 2A). The initial value of tail current (i_0) was plotted against the pulse potential (Fig. 2B). From extreme negative to extreme positive potentials, the curve displayed two phases, i_0 tending sigmoidally to a 'plateau' value (reached at about 0 mV) within the first phase, and then varying further towards zero within the second (Fig. 2B). Each of these two phases could reflect the voltage dependence of relative open probability (rel. p_{open}) of each of the two AKT2 channel populations. Namely, type-1 AKT2 channels would be fully activated at very negative potentials and fully deactivated at positive potentials, while type-2 channels would show partial deactivation only at potential values positive to +50 mV and would probably be fully deactivated at strongly positive potentials. This logical deduction from the initial hypothesis is further illustrated in Fig. 2C, where data were gathered from five cells displaying $r_{-140\,mV}$ values ranging from 53 to 88%. i_0 data obtained for a stimulation in the −180 mV to 0 mV range and those obtained for a stimulation in the 0 mV to +140 mV range were analysed separately. Whatever the $r_{-140\,mV}$ value, a single pair of Boltzmann curves, with apparent gating charges of 0.46 and 0.33 and midpoint found at −143 mV and +222 mV for type-1 and type-2, respectively, acceptably fitted rel. p_{open} data (see Section 2). The two rel. $p_{open}(E)$ terms obeying Boltzmann's law and being denoted *B1* and *B2*, it was checked that the biphasic curves shown in Fig. 2B could be fitted by $(1-r_{abs.})*B1+r_{abs.}*B2$, with $r_{abs.}$ representing the absolute (i.e. at any voltage) proportion of type-2 channels in the AKT2 channel population (Fig. 2D): this yielded $r_{abs.}$ values of 30, 59 and 80%. The $r_{-140\,mV}$ parameter introduced above was an underestimation of $r_{abs.}$ because type-1 channels are only partially activated at −140 mV. In turn, the $r_{abs.}$ and the Boltzmann parameters obtained in Fig. 2C,D respectively allowed to estimate the $r_{-140\,mV}$ parameter values for the three cells shown in Fig. 2A. This yielded 52, 78 and 91%, $r_{-140\,mV}$ values very similar to those obtained graphically from the raw data of Fig. 2A.

3.3. Two types of gating at the single-channel level

If the population of AKT2 channels actually sub-divides into two sub-populations, this should be observed at the single-channel level. In order to check the relevance of the ad hoc hypothesis stated above, further experiments were performed in conditions allowing recording of AKT2 unitary currents. Patch-clamp experiments on oocytes were performed in the cell-attached configuration because channel activity was invariably lost upon patch excision. Multi-channel patches (Fig. 3A–C) as well as single-channel patches (Fig. 3D–G) could be obtained. Histogram amplitudes (not shown) yielded a single value of unitary current, ≈2.3 pA at −100 mV, well in line with the unitary conductance of 22–25 pS reported previously for AKT2 [16,17]. Repeated 1.6 s pulses from a 0 mV holding potential to −100 mV were applied to multi-channel patches and subsequently averaged to yield pseudo-macroscopic current traces. A typical result is shown in Fig. 3A (201 records averaged) and compared to a macroscopic current trace obtained in a two-electrode voltage-clamp experiment. Similar time courses of both traces further support that the ≈2.3 pA unitary current denoted AKT2 activity. Analysing the pulses in deeper detail revealed an interesting feature. Although the unitary current amplitude was always the same, two different kinds of openings were observed: short openings with a mean open time of about 40 ms (Fig. 3B, left) and long openings of a duration apparently longer than 1.6 s, which were frequently interrupted by very short (< 3 ms) flickering closing events (Fig. 3B, middle). The 201 pulses were then sub-grouped in three categories: (I) 112 traces with only short openings (Fig. 3B, left), (II) 24 traces with only long openings (Fig. 3B, middle) and (III) 65 traces where the two types of openings were observed in the same pulse interval (Fig. 3B, right). The average of category I pulses displayed time-dependent activation kinetics but lacked any instantaneous component (Fig. 3C, left). The average of category II pulses displayed the instantaneous component but lacked any time-dependent activation kinetics (Fig. 3C, middle). The average of category III pulses displayed both an instantaneous and a time-dependent component (Fig. 3C, right). As suggested by macroscopic current analyses (Fig. 2), the two kinetic components of the AKT2 current would therefore correspond, at the single-channel level, to two different gating modes: a 'mode 1' resulting in short openings at −100 mV (Fig. 3C, left) and a 'mode 2' resulting in long openings at −100 mV (Fig. 3C, middle). Thus, two sub-populations of AKT2 channels would actually co-exist in the membrane.

In the following, two alternatives are considered, which

←

Fig. 3. Separation of two gating components of AKT2 at the single-channel level. A: Average of 201 current traces recorded on a multi-channel patch (cell-attached configuration, upper trace) compared to a macroscopic current trace obtained by two-electrode voltage-clamp experiments on an AKT2-expressing *Xenopus* oocyte (lower trace). In both cases, currents were evoked by 1.6-s-long voltage steps to −100 mV from a holding potential of 0 mV. External standard solution was composed of 100 mM KCl, 1 mM $CaCl_2$, 1.5 mM $MgCl_2$, 10 mM HEPES, pH 7.4 (NaOH). Pipettes were filled with 3 M KCl (two-electrode voltage-clamp) or with 100 mM KCl, 1 mM $CaCl_2$, 1.5 mM $MgCl_2$, 10 mM HEPES, pH 7.4 (NaOH) (cell-attached). B: Representative examples of the three categories of current traces obtained within the whole set of 201 traces. Left: One of the 112 traces showing short openings only; middle: one of the 24 traces showing long openings only; right: one of the 65 traces showing both types of opening (small arrows indicate short openings). C: Average of each category of traces shown in (B). D: 60-s-long segment of a gap-free record obtained at −40 mV on a single-channel patch showing a transition from gating mode 1 to gating mode 2. White symbols cross-refer to rel. p_{open} values plotted in (G). E: 10-s-long segments of a gap-free record obtained at different potential values on a single-channel patch gating either in mode 1 (two traces at top) or in mode 2 (three traces at bottom). Black symbols cross-refer to rel. p_{open} values plotted in (G). F: Values of unitary current obtained in same conditions as (D) and (E) plotted against potential. Circles and squares indicate, respectively, data from gating mode 1 and from gating mode 2. G: Rel. p_{open} in the patches shown in (D) (white) and (E) (black) plotted against voltage. The lines represent the rel. p_{open} (E) curves obtained in Fig. 2D. H: Proposed gating scheme for AKT2. The AKT2 channel population divides into two different fractions characterised by different gating modes. In mode 1, the gating is described by voltage-dependent transitions between several closed states (C) and the open state (O). In mode 2, the activation threshold is shifted to more positive values. In our experimental conditions with moderate voltages tolerated by the oocytes (−160 mV to +50 mV), a channel in mode 2 seems to be open all the time. The conversion of one channel from one mode into the other (figured by a ⇕) is under the control of – yet unknown – channel extrinsic factors.

have clearly different biophysical meanings: (i) a given channel belongs definitely to either type-1 or type-2 and (ii) any given channel can switch between the two gating modes. In the former situation, the above defined $r_{abs.}$ parameter represents the proportion of type-2 channels in the whole population, e.g. after irreversible post-transcriptional events resulting in expression of AKT2 channels of two types. In the latter situation, the $r_{abs.}$ value at steady-state has the meaning of a probability, namely the probability for any channel to gate in mode 2, i.e. to be of type-2; this may result from late and reversible post-translational events such as interaction with a cytosolic regulatory factor that could change the gating mode of the AKT2 channel. It is worth noting that the two gating modes were always observed in all studied patches. For instance, in the experiment displayed in Fig. 3A–C, the patch harboured channels showing the two gating modes. Up to three channels gating in mode 2 and up to two channels gating in mode 1 were observed simultaneously in some pulses. However in all the 201 pulses, never more than three channels were active at the same time. With respect to these data, the first of the two above alternatives would imply (i) that at least five channels co-existed in this patch (two of mode 1 and three of mode 2), (ii) that they never opened all at the same time (none of the 65 category-III records showed more than three channels open), (iii) that the mode 1 channels remained silent in all the 24 category-II records and (iv) that the mode 2 channels remained silent in all the 112 category-I records.

To obtain further lines of evidence for the ability of a given channel to switch between the two gating modes, gap-free records obtained on single-channel patches were analysed (Fig. 3D–G). In such records, transitions from one gating mode to the other were often observed. An example of transition from mode 1 to mode 2 at −40 mV is shown in panel D. During the phase in mode 1 (more than 49 s long), the rel. p_{open} was 0.014 at −40 mV. During the phase in mode 2 (more than 60 s long), rel. p_{open} was 0.96 at −40 mV. The white circle and the white square in panel G show that these rel. p_{open} values are in good agreement with the curves derived from macroscopic currents. 10-s-long segments of a gap-free record made on another patch are shown in panel E. These segments of record were selected before (Fig. 3E, top) and after (Fig. 3E, bottom) a clear transition from mode 1 and mode 2, such as the one shown in panel D. The effect of voltage on the channel is shown in both gating modes in panel E. At any studied potential, open time was much longer in mode 2 than in mode 1 (see above text relative to Fig. 3B). For instance, at +60 mV the channel never opened in mode 1 (not shown), while it showed long open and short closed times in mode 2 (Fig. 3E). Unitary current (i) and rel. p_{open} corresponding to sample records obtained in the −140 to +60 mV range are plotted against voltage in panels F and G, respectively (black circles: mode 1; black squares: mode 2). Analysis of mode 1 and mode 2 records yielded the same value for unitary current (at potential values negative to −40 mV; Fig. 3F). By contrast, rel. p_{open} values determined in each case were clearly different for mode 1 and mode 2 records and agreed well with the Boltzmann curves derived from the analyses of macroscopic currents recorded in COS cells (Fig. 3G).

3.4. Dual-gating mode of AKT2 channel: control by some unidentified post-translational event

Based on the whole set of observations, a model can be proposed accounting for the complex behaviour of AKT2. At a given time, the AKT2 channel population divides into two sub-populations. Some AKT2 channels gate in mode 1, the others in mode 2. The former channels display a voltage-gating behaviour within the commonly studied voltage range (half-activation potential in the −140 mV range), like the well-described KAT1 channel [24]. The gating of this fraction could be described by a multi-state scheme (Fig. 3H, mode 1). Mode 2 channels are also voltage-gated (rel. p_{open} at −40 mV > rel. p_{open} at +60 mV, see Fig. 3G), the half-activation potential being, however, far more positive (> +200 mV, see also Fig. 2), similar to that of the S4-mutant KAT1-S168R [25]. The gating of mode 2 channels might also be described by a multi-state scheme (Fig. 3H, mode 2). There must be, as suggested in the preceding section, some late and reversible post-translational events (figured by the vertical ⇔ in Fig. 3H) that affect the gating mode of AKT2 channels. Whether this may be an interaction with some cytoplasmic factor, which would result either in the binding of a cyclic nucleotide, a regulatory peptide, etc., or in a protonation, an oxidation, a phosphorylation event remains to be elucidated. Interestingly, Bockenhauer and coworkers recently reported an analogous change in gating mode of the animal KCNK2 channel: this TWIK-like (2-pore and K^+-selective) channel behaves as a leak channel when dephosphorylated and as a depolarisation-activated outward rectifier upon phosphorylation [26]. We are currently investigating a possible phosphorylation dependency of AKT2 channel operation.

Acknowledgements: We are grateful to Jossia Boucherez for expert technical assistance. Furthermore, we thank Isabel Lefevre for helpful comments and critical reading of the manuscript. This work was partly supported by the European Communities' BIOTECH Program (BIO4-CT96), by Rhône-Poulenc, and by a Marie-Curie Fellowship of the European Union to I.D. (Contract No. ERBBIO4CT985058, Proposal No. 980115).

References

[1] Anderson, J.A., Huprikar, S.S., Kochian, L.V., Lucas, W.J. and Gaber, R.F. (1992) Proc. Natl. Acad. Sci. USA 89, 3736–3740.
[2] Schachtman, D.P., Schroeder, J.I., Lucas, W.J., Anderson, J.A. and Gaber, R.F. (1992) Science 258, 1654–1658.
[3] Hedrich, R., Moran, O., Conti, F., Busch, H., Becker, D., Gambale, F., Dreyer, I., Küch, A., Neuwinger, K. and Palme, K. (1995) Eur. Biophys. J. 24, 107–115.
[4] Hoshi, T. (1995) J. Gen. Physiol. 105, 309–328.
[5] Véry, A.-A., Gaymard, F., Bosseux, C., Sentenac, H. and Thibaud, J.-B. (1995) Plant J. 7, 321–332.
[6] Pilot, G., Lacombe, B., Gaymard, F., Cherel, I., Boucherez, J., Thibaud, J.-B. and Sentenac, H. (2001) J. Biol. Chem. 276, 3215–3221.
[7] Müller-Röber, B., Ellenberg, J., Provart, N., Willmitzer, L., Busch, H., Becker, D., Dietrich, P., Hoth, S. and Hedrich, R. (1995) EMBO J. 14, 2409–2416.
[8] Sentenac, H., Bonneaud, N., Minet, M., Lacroute, F., Salmon, J.-M., Gaymard, F. and Grignon, C. (1992) Science 256, 663–665.
[9] Gaymard, F., Cerutti, M., Horeau, C., Lemaillet, G., Urbach, S., Ravallec, M., Devauchelle, G., Sentenac, H. and Thibaud, J.-B. (1996) J. Biol. Chem. 271, 22863–22870.
[10] Zimmermann, S., Talke, I., Ehrhardt, T., Nast, G. and Müller-Röber, B. (1998) Plant Physiol. 116, 879–890.
[11] Philippar, K., Fuchs, I., Lüthen, H., Hoth, S., Bauer, C.S., Haga, K., Thiel, G., Ljung, K., Sandberg, G., Böttger, M., Becker, D. and Hedrich, R. (1999) Proc. Natl. Acad. Sci. USA 96, 12186–12191.
[12] Hartje, S., Zimmermann, S., Klonus, D. and Müller-Röber, B. (2000) Planta 210, 723–731.

[13] Gaymard, F., Pilot, G., Lacombe, B., Bouchez, D., Bruneau, D., Boucherez, J., Michaux-Ferriere, N., Thibaud, J.-B. and Sentenac, H. (1998) Cell 94, 647–655.
[14] Ache, P., Becker, D., Ivashikina, N., Dietrich, P., Roelfsema, M.R. and Hedrich, R. (2000) FEBS Lett. 486, 93–98.
[15] Philippar, K., Fuchs, I., Lüthen, H., Hoth, S., Bauer, C.S., Haga, K., Thiel, G., Ljung, K., Sandberg, G., Böttger, M., Becker, D. and Hedrich, R. (1999) Proc. Natl. Acad. Sci. USA 96, 12186–12191.
[16] Marten, I., Hoth, S., Deeken, R., Ache, P., Ketchum, K.A., Hoshi, T. and Hedrich, R. (1999) Proc. Natl. Acad. Sci. USA 96, 7581–7586.
[17] Lacombe, B., Pilot, G., Michard, E., Gaymard, F., Sentenac, H. and Thibaud, J.B. (2000) Plant Cell 12, 837–851.
[18] Cao, Y., Ward, J.M., Kelly, W.B., Ichida, A.M., Gaber, R.F., Anderson, J.A., Uozumi, N., Schroeder, J.I. and Crawford, N.M. (1995) Plant Physiol. 109, 1093–1106.
[19] Ketchum, K.A. and Slayman, C.W. (1996) FEBS Lett. 378, 19–26.
[20] Uozumi, N., Nakamura, T., Schroeder, J.I. and Muto, S. (1998) Proc. Natl. Acad. Sci. USA 95, 9773–9778.
[21] Reyes, R., Duprat, F., Lesage, F., Fink, M., Salinas, M., Farman, N. and Lazdunski, M. (1998) J. Biol. Chem. 273, 30863–30869.
[22] Jurman, M.E., Boland, L.M., Liu, Y. and Yellen, G. (1994) BioTechniques 17, 876–881.
[23] Lacombe, B. and Thibaud, J.-B. (1998) J. Membr. Biol. 166, 91–100.
[24] Zei, P.C. and Aldrich, R.W. (1998) J. Gen. Physiol. 112, 679–713.
[25] Dreyer, I., Antunes, S., Hoshi, T., Müller-Röber, B., Palme, K., Pongs, O., Reintanz, B. and Hedrich, R. (1997) Biophys. J. 72, 2143–2150.
[26] Bockenhauer, D., Zilberberg, N. and Goldstein, S.A.N. (2001) Nat. Neurosci. 4, 1–6.